Reactivity of Small $Mo_xO_y^-$ Clusters toward Methane and Ethane

Richard B. Wyrwas, Bruce L. Yoder, Joshua T. Maze, and Caroline Chick Jarrold*

Indiana University, Department of Chemistry, 800 East Kirkwood Avenue, Bloomington, Indiana 47405

Received: December 9, 2005

The reactions of $Mo_2O_y^-$ suboxide clusters with both methane and ethane have been studied with a combination of mass spectrometry, anion photoelectron spectroscopy, and density functional theory calculations. Reactions were carried out under "gentle" and "violent" conditions. For methane, a number of products appeared under the gentler source conditions that were more logically attributed to dissociation of $Mo_2O_y^-$ clusters upon reacting with methane to form $MoCH_2^-$, $Mo(O)CH_2^-$, and $HMo(O_2)CH_3^-$. With ethane, products observed under the same gentle conditions were $Mo(O)C_2H_2^-$, $Mo(O)C_2H_4^-$, $Mo(O_2)C_2H_4^-$, and $Mo(O_2)(C_2H_5)_2^-$. As expected, more products were observed when the reactions were carried out under violent conditions. The photoelectron spectra obtained for these species were compared to calculated adiabatic and vertical electron affinities and vibrational frequencies, leading to definitive structural assignments for several of the products.

I. Introduction

Molybdenum oxide (MoO_3, molybdite) has been identified as one of several materials that may be used in the catalytic oxidation of methane for the production of methanol[1−4] or as a source for petrochemical feedstocks.[5−7] Apart from being intermediates in molybdite particle formation and F-center defect sites, molybdenum centers in lower-than-bulk oxidation states ("suboxides") are intriguing due to their role in the Mars−van Krevelen mechanism of catalytic oxidation,[8] which involves transfer of oxygen from bulk MoO_3 to the organic substrate followed by reoxidation of the catalyst by ambient O_2. This action results in crystallographic shearing forming *suboxide* particles.[9] Goddard and co-workers have performed computational studies of methane activation by chromium, molybdenum, and tungsten oxide clusters in which MO_2 (M = Cr, Mo, and W) suboxide species emerged as the most favorable candidates for oxidative addition of methane to the cluster.[10] Additionally, MoO_3 enhances NO reduction when added to standard materials found in catalytic converters,[11,12] which stimulated theoretical studies by Friend and co-workers that predicted that NO adsorbs to MoO_3 surfaces at oxygen *vacancies*.[13] So, in a wide range of theoretical studies, molybdenum atoms in suboxide states have been emerging as important defect sites on which catalytic activity may be localized.

While studies of suboxide defect sites in bulk materials are challenging, progress has been made in recent years in the study of transition metal oxide cluster reactivity.[14−23] Since bonding in metal oxides tends to be highly localized, cluster properties will more closely reflect bulk properties. Very little experimental work is available on the Cr/Mo/W series,[24−31] particularly for the negative ions, which may in fact be more relevant under applied conditions, since negative charge accumulation on surfaces is expected.[32]

As a first step in probing the interactions between small molybdenum suboxide cluster anions and methane and ethane, we have measured the reactivity of small molybdenum oxide cluster anions toward methane and ethane under two distinct reaction conditions and have determined the anionic products using mass spectrometry. A surprising observation is that complexes with a single molybdenum atom appear to result from reactions between larger clusters and the alkane. The photoelectron (PE) spectra of the more prominent products containing a single molybdenum atom have therefore been measured and are the focus of this paper. Computational studies on the cluster structures and their reaction complexes facilitate interpretation of the spectra.

PE spectroscopy is amenable to these studies, since it allows for mass specific spectroscopic interrogation of the electronic properties of both the anion and neutral involved. Anion PE spectroscopy has been used to determine the electronic properties and structures of a wide range of atomic metal clusters,[33−37] binary metal clusters,[38−40] metal oxides[27,41−43] (many diatomics[44−52]), and metal sulfides.[53] Our group has used it to determine the structures of tin clusters[54] and their association reaction products with CN^- and CH_2CN^-,[55] the unsaturated reaction products between the nickel group atoms with several small organic molecules (methanol, ethylene, acetonitrile),[56−58] several aluminum oxide clusters along with their reaction products with water,[59−61] and small molybdenum oxide clusters.[62]

II. Methods

A. Experimental Details.

Molybdenum oxide cluster production, subsequent gas-phase reactions, mass spectrometric analysis of the products, and anion photoelectron spectra of the bare clusters and a number of the reaction complexes were all done using an apparatus described in detail previously.[59] Briefly, molybdenum oxide cluster anions are generated using a laser ablation−pulsed molecular beam valve source similar to that developed by Dietz and co-workers.[63] The source used in previous studies has been modified to accommodate the powder form in which isotopically pure ^{96}Mo (Trace Sciences International Corp.) and ^{98}Mo (Oak Ridge National Laboratory, Isotope Business Office) are avail-

* To whom correspondence should be addressed. E-mail: cjarrold@indiana.edu.

10.1021/jp057195n CCC: $33.50
Published on Web 01/21/2006

able. These particular isotopes were chosen because they were the least expensive from the respective suppliers.

Clusters are produced when the surface of a pressed Mo powder disk is ablated with the focused, second harmonic output (532 nm, 10 mJ/pulse) of a Nd:YAG laser operated at 30-Hz repetition rate. The laser pulse is synchronized with the arrival of the high-pressure gas pulse from the pulsed molecular beam valve with 100 psig stagnation pressure (either ultrahigh purity helium or a mixture of He and methane or ethane). Oxygen within the Mo sample was adequate to produce a distribution of metal oxide cluster anions. The resulting plasma passes from the 3-mm diameter source channel through a 15-mm long, 2-mm diameter clustering channel where clusters coalesce and cool. The mixture then passes through a 1-mm aperture into a 25-mm long, 4-mm diameter reaction region. The exit of the reaction region is choked to 2 mm to increase retention time and the total pressure in the reactor region. The gas mixture expands into a vacuum chamber and passes through a 3-mm diameter skimmer. Anions are selectively accelerated to 1 keV into a 1.2-m beam modulated time-of-flight mass spectrometer.[64,65]

Prior to colliding with an ion detector, the ion of interest (either bare or reaction complexes) is selectively photodetached using the second harmonic (532 nm, 2.33 eV) or third harmonic (355 nm, 3.49 eV) output of a second Nd:YAG laser at the intersection of the ion beam and a second, 1-m field-free drift tube situated perpendicular to the ion beam. A small fraction (10^{-4}) of the photoelectrons travels up this drift tube and collides with a dual microchannel plate detector. The electron drift times are recorded using a digitizing oscilloscope and averaged for 200 000 to 500 000 laser shots. The drift times of the photoelectrons are converted to binding energy ($BE = h\nu - e^{-}KE$) binned into 2-meV increments. The apparatus is calibrated frequently during data acquisition by obtaining the PE spectra of O^{-}, OH^{-}, and I^{-}, all of which have well-known electron affinities (EA). Spectra are collected with the electric field vector of the laser both parallel and perpendicular to the direction of electron detection for all species, though in all cases below, parallel polarization gave the most intense electron signal, consistent with detaching electrons from d-like molecular orbitals.

The resolution of the apparatus is 7 meV at $e^{-}KE = 0.5$ eV and deteriorates with $e^{-}KE$. In most cases, strong thermionic emission is observed at very low electron kinetic energies, which has been observed previously in small cluster anion detachment studies.[66] With the development and application of PE imaging techniques by Sanov[67] and Neumark,[68] observation of a large contribution from thermionic emission in photodetachment spectra is becoming more common.

Reactivity studies were performed under two different conditions: (1) The reactant (2−5% of methane or ethane) was seeded into the first molecular beam valve, so it is present in the ablation region during cluster formation, and (2) the reactant (10−15% methane or ethane in He) is directly injected into the reactant region using a second pulsed molecular beam valve. Heating from the solenoid beam valves was counteracted by cooling the source to a typical temperature near 240 K. The complexes generated via method (2) were subsequently studied using PE spectroscopy.

B. Computational Details.

Calculations were performed using the Gaussian 03 suite of electronic structure programs.[69] The structures of numerous isomers of the anion and neutral and $MoO_{1,2,3}$ clusters with methane and ethane complexes were optimized separately using B3LYP/SDD (keyword: extrabasis) and found to be minima on the potential-energy surface. These minima were verified by subsequent harmonic frequency calculations.

An extensive study of cluster symmetries and multiplicities was conducted on the optimized structures. The neutral Mo atom has a $5s^14d^5$ ($^7S_3$) ground-state occupancy. High-spin states in the clusters and complexes are therefore possible, and often favorable. The B3LYP hybrid density functional composed of Becke's three-parameter exchange functional[70] and Lee, Yang, and Parr's correlation functional[71,72] was chosen based on its reliability when tested on bare MoO_3^{-} and MoO_3, relative to the vibrationally resolved photoelectron spectrum.[62] For singlet spin multiplicities, the restricted method (RB3-LYP) was used, and for all higher spin states the spin-unrestricted method (UB3-LYP) was used. As with our calculations on $M_2O_y^{-}/M_2O_y$ clusters, the Stuttgart Dresden (SDD)[73−76] relativistic pseudopotential and the corresponding double-ζ basis set was used as a starting point. Pseudopotentials increase computational efficiency by forming an effective core potential (ECP) that represents the core electrons of an atom. In the case of molybdenum, 28 core electrons are incorporated into its pseudopotential and the remaining 14 electrons are treated explicitly. Geometric optimizations were performed using the corresponding SDD basis for all atoms (Mo, O, C, and H) in the clusters. After obtaining the "most competitive" structures energetically for a given stoichiometry, extra basis functions were manually added on all atoms. In the case of Mo, an extra-diffuse function for the s, p, and d orbitals, as well as a polarization function to describe the f orbital was placed in the basis. For O and C, diffuse S and P functions were added along with a polarization D function. Hydrogen was given a diffuse S function and polarization P function. Diffuse functions were obtained by applying a 0.3 contraction factor, and polarization functions were taken from the 6-311++G** basis set.[77]

We calculated all one-electron-accessible excited neutral states using time-dependent density functional theory (TD DFT).[78−80] Adiabatic electron affinities were calculated by the zero-point-corrected energy difference between the optimized anion and its corresponding optimized neutral structure. Vertical detachment energies were determined by performing single point calculations on the optimized geometry of the anion with the charge and multiplicity of the neutral species.

Finally, the free energies of numerous hypothetical reactions ($\Delta_f G^{\theta}$), were tabulated for cluster anions, neutrals, and a number of known and possible reaction products in order to determine the free energies of various reactions possibly occurring in the experiment. $\Delta_f G^{\theta}$ was calculated at 250, 298.15, and 500 K.

III. Results and Analysis

A. Mass Spectra.

A typical mass spectrum of $^{96}Mo_xO_y^{-}$ ($x = 1-4$) generated with the source described above is shown in Figure 1. Note that, for each value of x, a distribution of y values is observed and no bare molybdenum cluster anions are present. Since ^{96}Mo has a mass equal to 6 oxygen atoms, peak assignments for $Mo_3O_{y\geq 8}^{-}$ and $Mo_4O_{y\leq 4}$ are ambiguous. However, the focus here is on the reactivity of smaller species, with particular attention paid to the reaction products containing a single molybdenum atom. Analysis of the larger cluster complexes will be presented in a later paper.

Methane Reactivity. Figure 2 shows a series of mass spectra in the $x = 1$ and 2 cluster size range obtained under different conditions. Panel a shows the product distribution when methane is seeded into the carrier gas (reaction condition 1). The solid

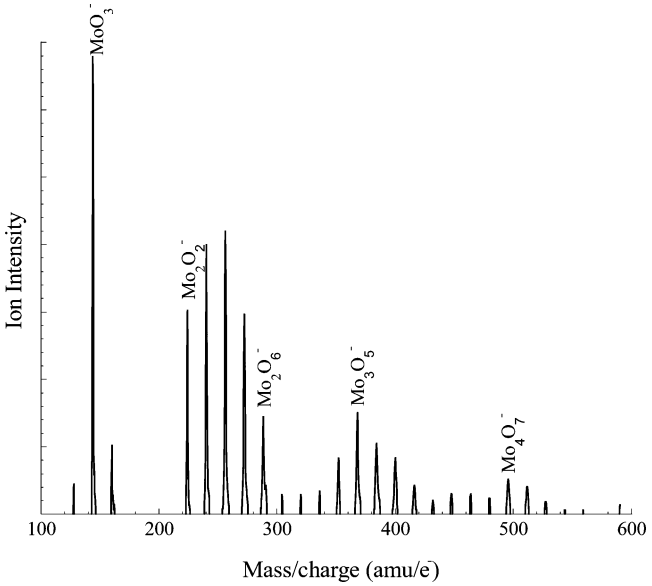

Figure 1. Typical mass spectrum of $^{96}Mo_xO_y^-$ clusters obtained using the cluster source described in the text.

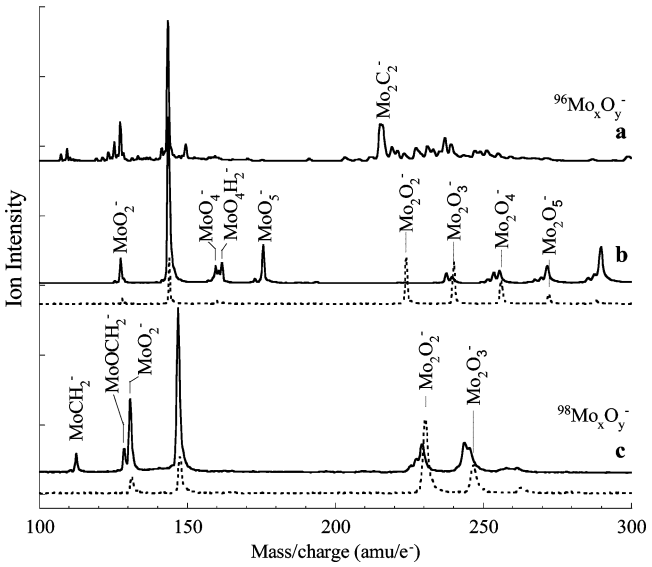

Figure 2. Mass spectra of molybdenum oxide anion complexes resulting from (a) reaction with methane in the ablation region of the cluster source, (b) methane introduced to flow reactor with higher $Mo_2O_y^-$ oxides present at −25 °C, and (c) methane in flow reactor with lower oxides present at −25 °C (dotted traces are pre-reaction cluster distributions).

traces in parts b and c of Figure 2 show product distributions resulting from injecting 15% methane in helium directly into the reaction channel (reaction condition 2). The difference between parts b and c of Figure 2 lies in the pre-reaction $Mo_xO_y^-$ cluster distributions, which are shown as dashed traces in parts b and c of Figure 2. In Figure 2b, $Mo_2O_y^-$ ($y = 4$, 5, and 6) clusters are more abundant than in Figure 2c, which has very little $y = 4$ and virtually no $y = 5$ and 6. We note here that, in Figure 2c, the ^{98}Mo isotope is used.

When methane is present in the laser ablation region (Figure 2a), molybdenum carbides, along with numerous partially dehydrogenated molybdenum oxide/methane complexes, are observed. The product distribution is simplified dramatically when the methane is added directly to the reaction channel. However, a common theme observed in all cases is that there is a considerable drop in the intensity of the $Mo_2O_y^-$ manifold

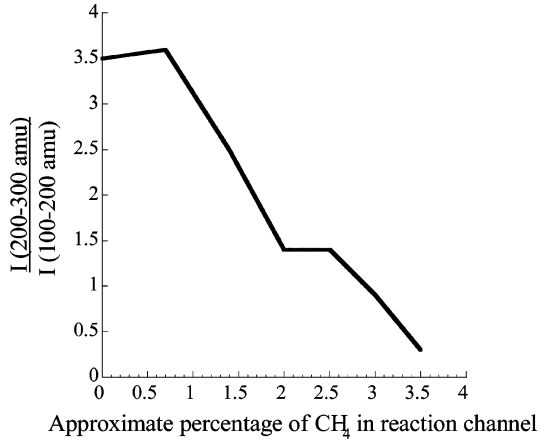

Figure 3. Relative integrated intensities of the $Mo_2O_y^-$ mass range to the MoO_y^- mass range as CH_4 concentration in the reaction channel is increased.

coupled with a large increase in the MoO_y^- manifold. Figure 3 shows the integrated intensities of the $x = 2$ manifold (200−300 amu) drops relative to the integrated intensities of the $x = 1$ (100−200 amu) manifold as the concentration of methane in the reaction channel is increased. While this may suggest that methane inhibits larger cluster formation, there is also a possibility that the larger clusters fragment upon reacting with one or more methane molecules to form complexes having single Mo atoms.

Different reaction products are observed for different cluster oxidation distributions. When higher oxides are present in the ion beam, the important product ions have masses corresponding to $MoO_2CH_4^-$, MoO_4^-, MoO_4H^-, and $MoO_4H_2^-$ and MoO_5^-. When little or no higher oxides are present in the beam, the important product ions are $MoCH_2^-$, $MoOCH_2^-$, and $MoO_2CH_4^-$. As mentioned before, increases in MoO_2^- and MoO_3^- intensities are also observed. Reaction products and their relative intensities with lower oxidation states under reaction conditions 1 and 2 are summarized in Table 1.

Ethane Reactivity. Figure 4 shows a series of mass spectra in the $x = 1$ and 2 cluster size region. As above, Figure 4a shows the mass distribution obtained when ethane is seeded in the carrier gas (reaction condition 1). The solid traces in parts b and c of Figure 4 show the product distribution when ethane is introduced in the reaction channel (reaction condition 2) given the two initial oxide conditions, shown as dotted traces. Figure 4b shows a higher oxide distribution than Figure 4c. The higher oxides again appear to enhance the number of products observed; $MoOC_2H_2^-$, $MoOC_2H_4^-$, $MoO_2C_2H_4^-$, and $MoO_2C_4H_{10}^-$ being the most dominant of the complexes observed within the MoO_y^- mass manifold. Consistent with the methane reactivity, a loss of intensity of the $Mo_2O_y^-$ manifold relative to the MoO_y^- manifold is observed, and reaction condition 1 yields a much more congested product distribution than condition 2. The peak assignments and relative abundances generated under the two different source conditions are also summarized in Table 1.

B. PE Spectra and Computational Results.

The PE spectra and lowest-energy structures calculated for the most important product ions observed under gentler reaction condition 2 with methane are shown in Figures 5 and 6, respectively. Figures 7 and 8 are analogous for reaction products with ethane. The calculated adiabatic electron affinity (EA_a) and vertical electron affinity (EA_v) for the lowest energy structural isomers found for these species are summarized in Table 2. We now consider the spectra and calculations in order of increasing mass, starting with the methane-based products.

TABLE 1: Relative Abundances of Clusters and Complexes Observe in Mass Spectra

			CH_4 (1)	CH_4 (2)	C_2H_6 (1)	C_2H_6 (2)
mass	assignment	helium	Figure 3a	parts b and c of Figure 3	Figure 4a	parts b and c of Figure 4
110	$MoCH_2^-$		0.08			
124	$MoCO^-$ or $MoC_2H_4^-$		0.06		0.08	0.05
126	$MoOCH_2^-$		0.13	0.03		
128	MoO_2^-	0.20	0.28	0.16	0.40	0.113
138	$MoOC_2H_2^-$				0.61	0.23
140	$MoOC_2H_4^-$				0.74	0.27
144	MoO_3^- and $MoO_2CH_4^-$	1.00	1.00	1.00	1.00	1.00
156	$MoO_2C_2H_4^-$				0.94	0.58
160	MoO_4^- and/or $MoO_3CH_4^-$	0.11	0.03	0.14	0.20	0.03
162	$MoO_4H_2^-$			0.15		
176	MoO_5^- and/or $MoO_3(CH_4)_2^-$			0.24		
186	$MoO_2(C_2H_5)_2^-$				0.28	0.46

Methane-Based Complexes: $MoCH_2^-$, $MoOCH_2^-$, MoO_2^-, and $MoO_2CH_4^-$.

1. $MoCH_2^-$. $MoCH_2^-$ is produced in large quantities only when $Mo_2O_y^-$ ($y \geq 4$) are very low in abundance. Figure 5a shows the PE spectra obtained using 2.33-eV (upper trace) and 3.49-eV (lower trace) photon energies. Metal$-CH_2^+$ complexes are frequently observed in reactions between transition metal atomic cations and methane.[81] The PE spectra exhibit a fairly sharp origin at 0.770(15) eV, taken to be the EA_a, with a broader shoulder with a maximum at 0.957(15) eV, or 1510(120) cm^{-1} to higher binding energy. The 2.33 eV spectrum clearly shows another vibrationally resolved electronic transition at 2.031(5) eV, with a 522(30)-cm^{-1} progression. The 3.49-eV spectrum shows another relatively sharp transition at 3.163(10) eV.

Calculations on this complex predict two close-lying structural isomers for the anion, shown in Figure 6, which include a $^4B_1$ ($^5B_1$ neutral analogue ground state) C_{2v} $MoCH_2^-$ structure and a $^4A''$ ($^3A''$ neutral ground state) C_s $HMoCH^-$ structure predicted to lie within 0.10 eV of the C_{2v} structure. Both structures are predicted to have low EA_a values (0.75 and 0.98 eV for the C_{2v} and C_s structures, respectively). However, for $MoCH_2^-$, the anion and neutral are predicted to be virtually structurally identical, resulting in a sharp PE spectrum. The $HMoCH^-$ structure, in contrast, is predicted to have a large change in Mo$-$C$-$H bond angle (129.54° in the anion to 93.68° in the neutral), with virtually no Franck$-$Condon overlap at the origin. We therefore assert that the lowest-energy transition observed in the spectrum is due to the $MoCH_2^-$ isomer but that the broad, unresolved signal to higher binding energy may be due to the competitive $HMoCH^-$ structure.

2. $MoOCH_2^-$. The PE spectrum of $MoOCH_2^-$ shows one distinct, broad electronic transition originating at 1.84(2) eV, with band maximum at 2.02(2) eV. There is a partially resolved, complex vibrational structure in this band. The calculations again predict two close-lying structural isomers for the anion, shown in Figure 6, one of which can be described as $Mo(O)CH_2^-$ ($^4A''$ anion and $^5A'$ neutral ground states) and the other as $HMo(O)CH^-$ (^2A anion and ^1A neutral ground states). The adiabatic electron affinities calculated for the $Mo(O)CH_2^-$ and $HMo(O)CH^-$ structures are, respectively, 2.53 eV ($EA_v = 2.87$ eV) and 1.99 eV ($EA_v = 2.20$ eV). The values for $HMo(O)CH^-$ are in better

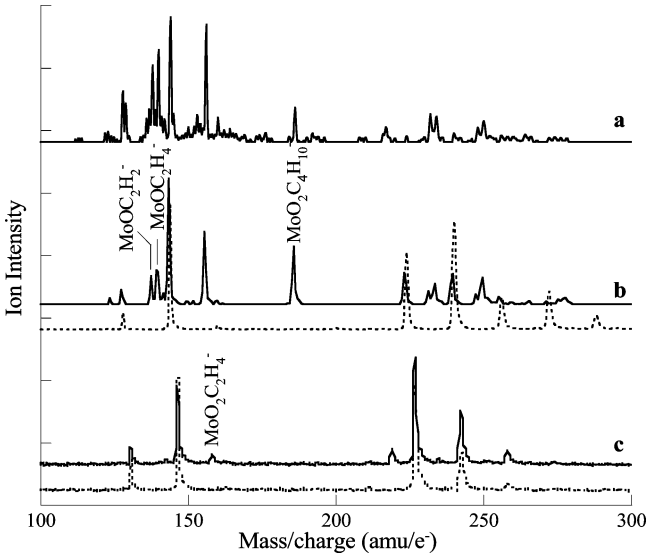

Figure 4. Mass spectra of molybdenum oxide anion complexes resulting from (a) reaction with ethane in the ablation region of the cluster source, (b) ethane introduced to flow reactor with higher $Mo_2O_y^-$ oxides present at $-$ 25 °C, and (c) ethane in flow reactor with lower oxides present at $-$25 °C (dotted traces are pre-reaction cluster distributions).

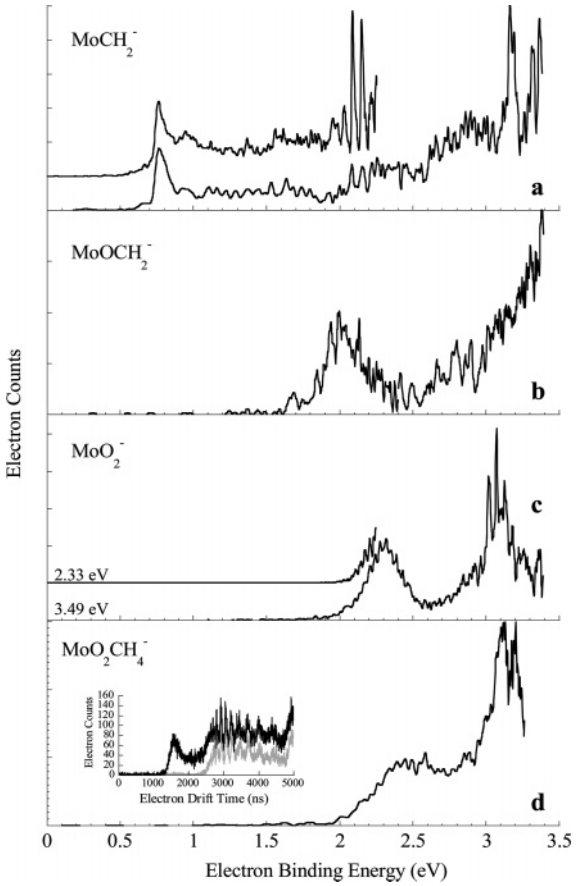

Figure 5. PE spectra of methane-based reaction complexes obtained using 3.49-eV photon energy.

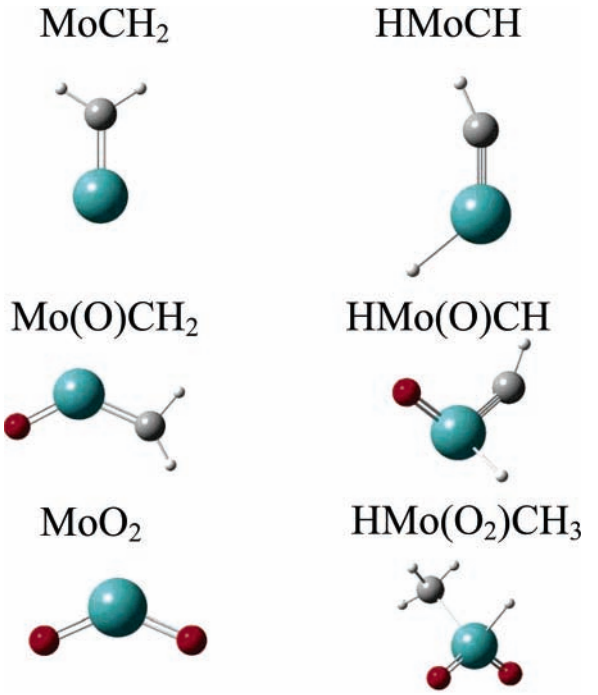

Figure 6. Lowest-energy structural isomers determined for the reaction complex anions observed in low-temperature reactions between $Mo_xO_y^-$ and methane.

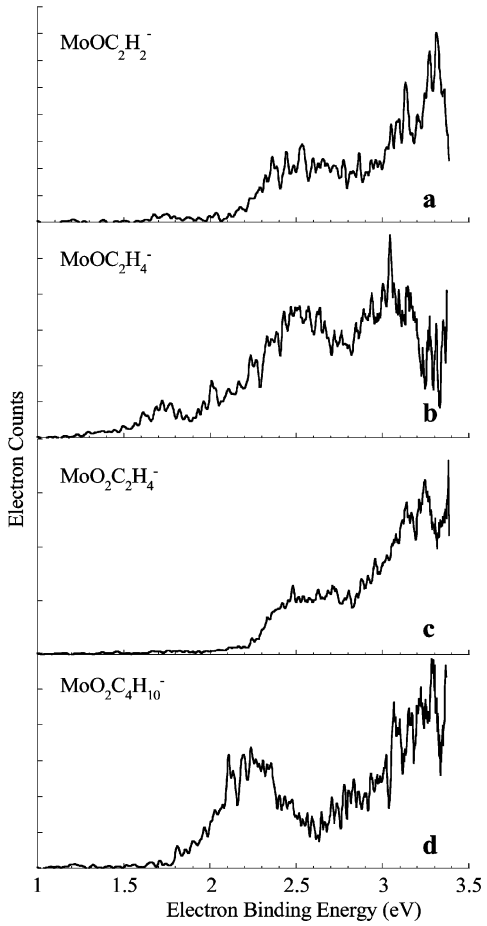

Figure 7. PE spectra of ethane-based reaction complexes obtained using 3.49 eV photon energy.

agreement with the spectrum. While the $HMo(O)CH^-$ structure is predicted to lie 0.04 eV higher in energy than the $Mo(O)CH_2^-$ structure, simulations based on the calculations (not shown)

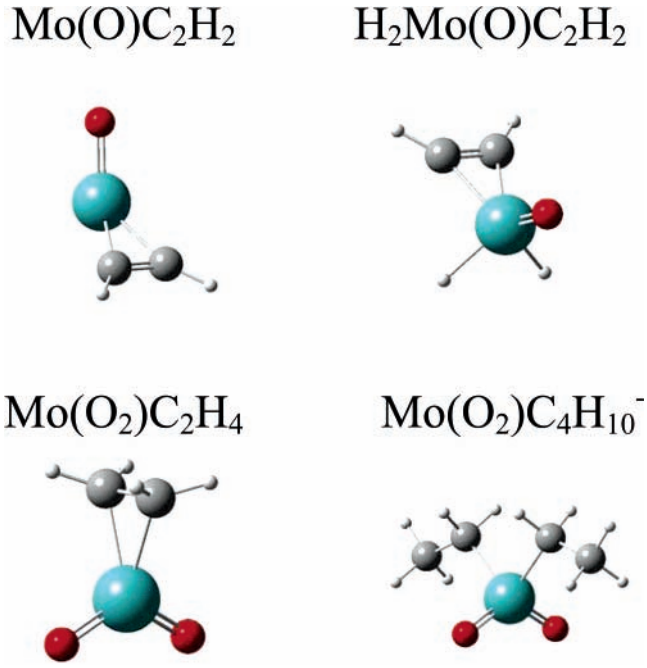

Figure 8. Lowest-energy structural isomers determined for the reaction complex anions observed in low-temperature reactions between $Mo_xO_y^-$ and ethane.

TABLE 2: Summary of Adiabatic and Vertical Electron Affinities Calculated for the Important Product Ions

anionic molecule/structure	rel anion energy (eV)	transition	EA_a (eV)	EA_v (eV)
$H-MoCH^-$	+0.09	$^3A'' \leftarrow {}^4A''$	0.91	1.56
$MoCH_2^-$	0	$^5B_1 \leftarrow {}^4B_1$	0.79	0.79
$H-Mo(O)CH^-$	+0.04	$^1A \leftarrow {}^2A$	1.99	2.20
$Mo(O)CH_2^-$	0	$^5A' \leftarrow {}^4A''$	2.53	2.87
$HMo(O_2)CH_3^-$	0	$^1A' \leftarrow {}^2A'$	2.06	2.57
MoO_2^-	0	$^3B_1 \leftarrow {}^4B_1$	2.15	2.41
$Mo(O)C_2H_2^-$	0	$^3A \leftarrow {}^4A''$	1.71	1.88
$H_2Mo(O)C_2H_2^-$	0	$^1A' \leftarrow {}^2A'$	2.10	2.60
$Mo(O_2)C_2H_4^-$	0	$^1A_1 \leftarrow {}^2A_1$	2.44	2.56
$Mo(O_2)C_4H_{10}^-$	0	$^1A' \leftarrow {}^2A_1$	1.69	2.27

support the hydride, $HMo(O)CH^-$ structure, with the most active mode being the hydride bend at 438 cm^{-1}.

3. MoO_2^-. The spectrum of MoO_2^- was included in Figure 5c because (i) the MoO_2^- ion signal was enhanced when the molybdenum oxide clusters were exposed to CH_4 and C_2H_6, (ii) the PE spectrum of MoO_2^- to our knowledge has not yet been published, and (iii) to determine whether the $MoOCH_4^-$ ion, which has a coincident mass with MoO_2^-, was also present in the beam. The 2.33- and 3.49-eV PE spectra, shown in Figure 5c, show a broad, partially vibrationally resolved transition with an onset of signal at 1.833 eV, the first distinct peak in the vibrational progression at 2.107 eV, and the band maximum at 2.317 eV. The calculated EA_a and EA_v, 2.15 and 2.41 eV, respectively, are in very good agreement with the experimental values. The characteristic vibrational spacing is 285(10) cm^{-1}, with a combination band fit with 965(30) cm^{-1}. These are close to the calculated bend and stretch frequencies of the bent, C_{2v} neutral $^3B_1$ structure, 299 and 1002 cm^{-1}, so this band is assigned to the $^3B_1 + e^- \leftarrow {}^4B_1$ transition. The structure of the $^4B_1$ anion is shown in Figure 6. The neutral bond angle, calculated to be 115.1°, is narrower than the anion bond angle, calculated to be 132.0°.

A vibrationally resolved excited-state transition is also observed with an origin at 3.02(1) eV and a vibrational spacing of 430(15) cm^{-1}. So far, we have not been able to calculate an

excited state in agreement with this band. The MoO_2^- spectrum exhibits this feature regardless of whether the methane (or ethane) is present, so it is not due to $MoOCH_4^-$.

4. $MoO_2CH_4^-$. The mass of $MoO_2CH_4^-$ coincides with MoO_3^-, and the inset of Figure 5d shows the raw electron count vs time spectra for pure MoO_3^- (gray trace) superimposed on the spectrum obtained from the 144-amu peak when methane was present in the reaction channel. The pure MoO_3^- signal was subtracted from the $MoO_2CH_4^-/MoO_3^-$ signal to obtain the spectrum shown Figure 5d.

The spectrum of $MoO_2CH_4^-$ shows a broad transition originating at 2.00(10) eV and a narrower excited state with the origin at 3.04(10) eV. The lowest-energy structure predicted for the anion and neutral, shown in Figure 6, is an insertion complex, $HMo(O_2)CH_3^-$, with anion ground state of $^2A'$ and a corresponding $^1A'$ neutral ground state. The calculated EA_a is 2.06 eV, with an EA_v of 2.56 eV. This is in very good agreement with the ground-state transition observed in the spectrum.

Ethane-Based Complexes: $MoOC_2H_2^-$, $MoOC_2H_4^-$, $MoO_2C_2H_4^-$, and $MoO_2C_4H_{10}^-$.

1. $MoOC_2H_2^-$. The PE spectrum of $MoOC_2H_2^-$ shown in Figure 7a shows at least three broad electronic bands originating at 1.7(1), 2.1(1), and 3.1(1) eV. Calculations on the possible isomers of this complex were difficult, with neutral structures in particular frequently failing to converge. However, convergence was achieved with the nonplanar triangular $Mo(O)C_2H_2^-$ structure, shown in Figure 8. The neutral ground state is predicted to be a ^3A and has lower symmetry than the corresponding $^4A''$ ground anion state. The EA_a is predicted to be 1.71 eV, with the EA_v at 1.88 eV. This coincides with the low-intensity signal found at lowest binding energy in the spectrum but is in poor agreement with the more intense signal, suggesting that the actual structures have not been found or that the neutral states accessed by detaching the anion are not structurally stable.

2. $MoOC_2H_4^-$. The anion PE spectrum of $MoOC_2H_4^-$ shown in Figure 7b is similar to $MoOC_2H_2^-$ and exhibits at least three broad, overlapping transitions originating roughly at 1.25(10), 1.9(1), and 2.9(1) eV. The lowest-energy anion corresponds to a double hydride $H_2Mo(O)C_2H_2^-$ structure, shown in Figure 8, which has a calculated EA_a of 2.10 eV and EA_v of 2.60 eV. These agree with the prominent central feature in the spectrum (1.9 eV origin) having a maximum at 2.45 eV. On the basis of the calculations, this broad transition can be attributed to relaxation of the −HMoH from 91.0° in the anion to 125.2° in the neutral and a contraction of the −CMoO from 120.7 to 108.0°. The most competitive isomer is a C−C insertion complex, $MoO(CH_2)_2^-$, which is calculated to be less stable by 0.38 eV.

3. $MoO_2C_2H_4^-$. The anion PE spectrum of $MoO_2C_2H_4^-$ shown in Figure 7c exhibits a transition with a sharp onset of electron signal observed at 2.25 eV, reaching a plateau at 2.5 eV, with additional peaks at 3.11 and 3.23 eV. The calculated ground-state anion and neutral structure for this complex is a C_{2v} $Mo(O_2)C_2H_4^-$ shown in Figure 8. It is essentially a MoO_2^- cluster bound to ethylene (−CMoC = ∼40°) out of the MoO_2 plane. The EA_a is calculated to be 2.44 eV, with the EA_v calculated to be 2.56 eV, both in good agreement with the observed spectrum. The first excited-state transition is predicted to lie at 3.16 eV, in agreement with the higher-lying structure in the spectrum.

4. $MoO_2C_4H_{10}^-$. The most prominent feature in the anion PE spectrum of $MoO_2C_4H_{10}^-$ shown in Figure 7d is an irregular band with a gentle onset of signal at 1.75(10) eV and a sharp rise in signal at 2.11(1) eV. The structure on this band is irregular but reproducible, with an initial spacing of 650(20) cm^{-1} (a 626-cm^{-1} symmetric mode is predicted for the neutral described below). The calculated ground-state anion structure is $Mo(O_2)(C_2H_5)_2^-$, described as a MoO_2 cluster with two C_2H_5 groups singly bound to the metal, shown in Figure 8. The EA_a for this isomer was calculated to be 1.69 eV with a EA_v of 2.27 eV, in good agreement with the observed spectrum.

IV. Discussion

A striking overall feature in the mass spectra shown in Figures 3 and 4 is the loss of intensity of the $Mo_2O_y^-$ accompanied by an increase in the MoO_y^- portion of the spectrum when the clusters are exposed to methane or ethane. In pure helium, the integrated intensities of the $Mo_2O_y^-$ clusters are considerably higher than the sum of the integrated intensities of the MoO_y^- clusters. This suggests that reactions between the larger clusters and the simple hydrocarbons in part result in fragmentation of the larger clusters, possibly because the reaction compromises the Mo−O−Mo bridge structures predicted for $Mo_2O_{y>2}^-$ clusters.[62] Furthermore, all of the complexes in the mass spectra obtained under gentler reaction conditions have two or fewer oxygen atoms, while MoO_2^- is sparce and MoO^- and Mo^- are absent in pure helium, which argues against MoO_2^- and MoO^- being dominant reaction species for the production of the observed complex ions. Additionally, we do not observe adducts for any dimolybdenum oxide cluster, other than $Mo_2O_2^-$, even as the relative partial pressure of methane and ethane are increased in the reactor. We do, however, find that higher-order single molybdenum oxides products, such as $MoO_2C_4H_{10}^-$, become more abundant as a function of increasing reactant partial pressure. The dependence of the product distribution on the abundance of the higher di-molybdenum oxides suggests that $Mo_2O_y^-$ clusters are the principle reactants for the products probed in this paper. Note, however, that $Mo_2O_5^-$ was very low in intensity and $Mo_2O_6^-$ was virtually absent in all the reactivity studies contained in this paper. Therefore, *suboxide* clusters with two molybdenum centers appear to be the main reactants.

Again, the focus here is on the products containing a single molybdenum atom. The mass spectra also reveal several products within the lighter end of the $Mo_2O_y^-$ manifold, which will be the focus of a subsequent study.

While the anionic products resulting from the cluster/methane or cluster/ethane reactions are determined definitively from the mass spectra, the reactants are not isolated from the cluster mixture prior to the reaction. However, based on the above observations, we can infer the nature of the reactions that are taking place. In the reactions with methane, we observed the appearance of, among other things, $MoO_2CH_4^-$. While a reaction such as $MoO_3^- + CH_4 \rightarrow MoO_2CH_4^- + O^\bullet$ may be occurring, our observations suggest reactions of the type

$$Mo_2O_y^- + nCH_4 \rightarrow MoO_2CH_4^- + MoO_{y-2}(n-1)(CH_4) \quad (y < 3x)$$

$$Mo_2O_y^- + nCH_4 \rightarrow MoOCH_2^- + H_2MoO_{y-1}(n-1)(CH_4) \text{ [or } MoO_{y-1}(n-1)CH_4 + H_2\text{]}$$

$$Mo_2O_y^- + nCH_4 \rightarrow MoCH_2^- + H_2MoO_y(n-1)CH_4 \text{ [or } MoO_y(n-1)CH_4 + H_2\text{]}$$

When higher oxides, stoichiometric or hyperoxides, are present in the $Mo_2O_y^-$ manifold, MoO_4^-, $MoO_4H_2^-$, and MoO_5^- are

produced. These complexes have considerably higher electron affinities than $MoCH_2$ and $MoOCH_2$ so the electron would remain with the oxides in reactions such as $Mo_2O_4^- + CH_4 \rightarrow MoCH_2 + MoO_4^- + H_2$. Note that both the $MoOCH_2^-$ and $MoCH_2^-$ involve loss of $2H^\bullet$ from methane (i.e., oxidation of the methane) evoking a picture of molecular hydrogen evolution. Neutral products are not detected in this experiment, so we cannot assert whether metal dihydride formation or molecular hydrogen formation is resulting in the reaction. However, recent work by Davis and co-workers showed that, in reactions between atomic molybdenum and 2-butyne, H_2 elimination was the sole reaction channel.[82]

We have explored the thermodynamics of some potential reactions between dimolybdenum oxide cluster anions and a single methane

$$Mo_2O_2^- + CH_4 \rightarrow MoO_2CH_4^- + Mo \quad \Delta G_{298} = +11.95 \text{ kcal/mol}$$

$$Mo_2O_3^- + CH_4 \rightarrow MoO_2CH_4^- + MoO \quad \Delta G_{298} = +39.26 \text{ kcal/mol}$$

$$Mo_2O_4^- + CH_4 \rightarrow MoO_2CH_4^- + MoO_2 \quad \Delta G_{298} = +50.74 \text{ kcal/mol}$$

We have obtained less unfavorable results by considering the double reaction of methane with the $Mo_2O_4^-$ cluster

$$Mo_2O_4^- + 2\,CH_4 \rightarrow MoO_2CH_4^- + MoO_2CH_4 \quad \Delta G_{298} = +22.84 \text{ kcal/mol}$$

We are presently investigating the addition of more than two CH_4s to a range of oxides.

The simplest reaction giving a spontaneous result is

$$MoO_2^- + CH_4 \rightarrow MoO_2CH_4^- \quad \Delta G_{298} = -26.16 \text{ kcal/mol}$$

Note, however, that MoO_2^- is never present in an appreciable amount in the ion beam.

The $MoO_2C_4H_{10}^-$ complex is unique in that it is the only complex observed that exhibits the addition of two ethane molecules. It is further interesting because no $MoO_2C_2H_5^-$ is observed though $MoO_2C_2H_4^-$ is abundant, suggesting that the residence time of the complexes in the source is long relative to the lifetime of the $MoO_2C_2H_5^-$ intermediate. The prevalence of the $MoO_2C_4H_{10}^-$ complex supports the hypothesis that the observed complexes may result from sequential alkane additions with the larger clusters. $Mo_2O_4^-$ has a double Mo−O−Mo bridge in its lowest-energy structure, it is conceivable that at least two reactions are required before fragmentation occurs.

We close the discussion section with two final observations. The complexes formed have simple, oxidized hydrocarbon ligands on an electron-rich metal center. It will be interesting to determine in subsequent reactivity studies whether these species can undergo electrophilic substitution reactions. With regard to common models of catalytic oxidation of hydrocarbons, it will also be interesting to determine if addition of oxygen in a sequential, isolated reaction region (to model ambient free molecular oxygen in an applied setting) will result in the release of alkoxy radical ions.

V. Conclusions

The combination of mass spectrometry, anion PE spectroscopy, and DFT calculations have revealed a class of reaction products involving $Mo_2O_y^-$ suboxide cluster fragmentation upon reaction with simple hydrocarbons. This is supported by the following observations: With exposure to methane or ethane under relatively gentle reaction conditions, a loss of $Mo_2O_y^-$ intensity is observed relative to the MoO_y^- intensity in mass distributions measured from a cluster source coupled to a reaction channel. Further, the reaction complexes formed generally have 0, 1, or 2 oxygen atoms, while MoO_y^- ($y = 2$, 1, 0) have low or no abundance in the ion source.

The complexes formed, which include $MoCH_2^-$, $Mo(O)CH_2^-$, and $Mo(O_2)CH_4^-$ in reactions with methane and $Mo(O)C_2H_2^-$, $Mo(O)C_2H_4^-$, $Mo(O_2)C_2H_4^-$, and $Mo(O_2)C_4H_{10}^-$ in reactions with ethane, suggest a rich set of chemical interactions involving C−H bond insertions, Mo−O−Mo bridge breaking, and molecular hydrogen evolution. The stable structures emerging from the DFT calculations show metal hydride formation as being favorable in the formation of $HMo(O_2)CH_3^-$ and, at a minimum, energetically competitive with $Mo{=}CH_2$ formation for both $MoCH_2^-/HMoCH^-$ and $Mo(O)CH_2^-/HMo(O)CH^-$. Metal−acetylene complexes were predicted for the $MoOC_2H_2^-$ and $H_2MoOC_2H_2^-$ ethane-based complexes, but no definitive structural assignment could be made based on the respective PE spectra. However, for both $Mo(O_2)C_2H_4^-$ and $Mo(O_2)(C_2H_5)_2^-$, the good agreement between the spectra and calculations suggest that MoO_2^- is the central feature with an ethylene ligand and two ethyl ligands, respectively.

Acknowledgment. The authors gratefully acknowledge the invaluable and generous help of Prof. Krishnan Raghavachari. This research was supported by National Science Foundation Grant No. CHE 0350193.

Supporting Information Available: Complex structures and thermochemical quantities calculated in these studies, along with the extra basis sets used, are available free of charge via the Internet at http://pubs.acs.org.

References and Notes

(1) Oyama, S. T.; Radhakrishnan, R.; Seman, M.; Kondo, J. N.; Domen, K.; Asakura, K. *J. Phys. Chem. B* **2003**, *107*, 1845.
(2) Machiels, C. J.; Sleight, A. W. *J. Catal.* **1982**, *76*, 238.
(3) Holstein, W. L.; Machiels, C. J. *J. Catal.* **1996**, *162*, 118.
(4) Kim, D. S.; Wachs, I. E.; Segawa, K. *J. Catal.* **1994**, *149*, 268.
(5) Wang, D.; Lunsford, J. H.; Rosynek, M. P. *Top. Catal.* **1996**, *3*, 289.
(6) Solymosi, F.; Cserenyi, J.; Szoke, A.; Bansagi, T.; Oszko, A. *J. Catal.* **1997**, *165*, 150.
(7) Zhang, W.; Oyama, S. T.; Holstein, W. L. *Catal. Lett.* **1996**, *39*, 67.
(8) Mars, P.; van Krevelen, D. W. *Chem. Eng. Sci.* **1954**, *3*, 41.
(9) Wang, D.; Su, D.; Schlogl, R. *Cryst. Res. Technol.* **2003**, *38*, 153.
(10) Xu, X.; Faglioni, F.; Goddard, W. A., III. *J. Phys. Chem. A* **2002**, *106*, 7171.
(11) Halasz, I.; Brenner, A.; Shelef, M. *Appl. Catal., B* **1993**, *2*, 131.
(12) Yao, H. C. *Appl. Surf. Sci.* **1984**, *19*, 398.
(13) Remediakis, I. N.; Kaxiras, E.; Chen, M.; Friend, C. M. *J. Chem. Phys.* **2003**, *118*, 6046.
(14) Bergeron, D. E.; Castleman, A. W., Jr.; Jones, N. O.; Khanna, S. N. *Nano Lett.* **2004**, *4*, 261.
(15) Bell, R. C.; Castleman, A. W., Jr. *J. Phys. Chem. A* **2002**, *106*, 9893.
(16) Briand, L. E.; Farneth, W. E.; Wachs, I. E. *Catal. Today* **2000**, *62*, 219.
(17) Burcham, L. J.; Deo, G.; Gao, X.; Wachs, I. E. *Top. Catal.* **2000**, *11/12*, 85.
(18) Chen, Y.; Wachs, I. E. *J. Catal.* **2003**, *217*, 468.
(19) Fialko, E. F.; Kikhtenko, A. V.; Goncharov, V. B.; Zamaraev, K. I. *J. Phys. Chem. A* **1997**, *101*, 8607.
(20) Fialko, E. F.; Kikhtenko, A. V.; Goncharov, V. B.; Zamaraev, K. I. *J. Phys. Chem. B* **1997**, *101*, 5772.
(21) Justes, D. R.; Mitric, R.; Moore, N. A.; Bonacic-Koutecky, V.; Castleman, A. W., Jr. *J. Am. Chem. Soc.* **2003**, *125*, 6289.

(22) Kimble, M. L.; Castleman, A. W. *Int. J. Mass Spectrom.* **2004**, *233*, 99.
(23) Waters, T.; O'Hair, R. A. J.; Wedd, A. G. *J. Am. Chem. Soc.* **2003**, *125*, 3384.
(24) Sun, Q.; Rao, B. K.; Jena, P.; Stolcic, D.; Kim, Y. D.; Gantefor, G.; Castleman, A. W., Jr. *J. Chem. Phys.* **2004**, *121*, 9417.
(25) Lightstone, J. M.; Mann, H. A.; Wu, M.; Johnson, P. M.; White, M. G. *J. Phys. Chem. B* **2003**, *107*, 10359.
(26) Aubriet, F.; Muller, J.-F. *J. Phys. Chem. A* **2002**, *106*, 6053.
(27) Sun, Q.; Rao, B. K.; Jena, P.; Stolcic, D.; Gantefor, G.; Kawazoe, Y. *Chem. Phys. Lett.* **2004**, *387*, 29.
(28) Zhai, H. J.; K., B.; Cui, L. F.; Li, X.; Dixon, D. A.; Wang, L.-S. *J. Am. Chem. Soc.* **2004**, *126*, 16134.
(29) Zhai, H. J.; H., X.; Cui, L. F.; Li, X.; Li, J.; Wang, L.-S. *J. Phys. Chem. A* **2005**, *109*, 6019.
(30) Gutsev, G. L.; Jena, P.; Zhai, H.-J.; Wang, L.-S. *J. Chem. Phys.* **2001**, *115*, 7935.
(31) Bauschlicher, C. W., Jr.; Gutsev, G. L. *J. Chem. Phys.* **2002**, *116*, 3659.
(32) Dungey, K. E.; Curtis, M. D.; Penner-Hahn, J. E. *Chem. Mater.* **1998**, *10*, 2152.
(33) Ho, J.; Ervin, K. M.; Lineberger, W. C. *J. Chem. Phys.* **1990**, *93*, 6987.
(34) McHugh, K. M.; Eaton, J. G.; Lee, G. H.; Sarkas, H. W.; Kidder, L. H.; Snodgrass, J. T.; Manaa, M. R.; Bowen, K. H. *J. Chem. Phys.* **1989**, *91*, 3792.
(35) Morenzin, J.; Kietzmann, H.; Bechthold, P. S.; Gantefor, G.; Eberhardt, W. *Pure Appl. Chem.* **2000**, *72*, 2149.
(36) Taylor, K. J.; Pettiette-Hall, C. L.; Cheshnovsky, O.; Smalley, R. E. *J. Chem. Phys.* **1992**, *96*, 3319.
(37) Wang, L. S.; Wu, H. *Z. Phys. Chem.* **1998**, *203*, 45.
(38) Koyasu, K.; Mitsui, M.; Nakajima, A.; Kaya, K. *Chem. Phys. Lett.* **2002**, *358*, 224.
(39) Negishi, Y.; Nakamura, Y.; Nakajima, A.; Kaya, K. *J. Chem. Phys.* **2001**, *115*, 3657.
(40) Pramann, A.; Nakajima, A.; Kaya, K. *J. Chem. Phys.* **2001**, *115*, 5404.
(41) Pramann, A.; Koyasu, K.; Nakajima, A.; Kaya, K. *J. Phys. Chem. A* **2002**, *106*, 4891.
(42) Pramann, A.; Koyasu, K.; Nakajima, A.; Kaya, K. *J. Chem. Phys.* **2002**, *116*, 6521.
(43) Pramann, A.; Nakamura, Y.; Nakajima, A.; Kaya, K. *J. Phys. Chem. A* **2001**, *105*, 7534.
(44) Fan, J.; Wang, L.-S. *J. Chem. Phys.* **1995**, *102*, 8714.
(45) Gunion, R. F.; Dixon-Warren, S. J.; Lineberger, W. C. *J. Chem. Phys.* **1996**, *104*, 1765.
(46) Klopcic, S. A.; Moravec, V. D.; Jarrold, C. C. *J. Chem. Phys.* **1999**, *110*, 10216.
(47) Moravec, V. D.; Jarrold, C. C. *J. Chem. Phys.* **1998**, *108*, 1804.
(48) Moravec, V. D.; Klopcic, S. A.; Chatterjee, B.; Jarrold, C. C. *Chem. Phys. Lett.* **2001**, *341*, 313.
(49) Polak, M. L.; Gilles, M. K.; Gunion, R. F.; Lineberger, W. C. *Chem. Phys. Lett.* **1993**, *210*, 55.
(50) Polak, M. L.; Gilles, M. K.; Ho, J.; Lineberger, W. C. *J. Phys. Chem.* **1991**, *95*, 3460.
(51) Wenthold, P. G.; Gunion, R. F.; Lineberger, W. C. *Chem. Phys. Lett.* **1996**, *258*, 101.
(52) Wu, H.; Desai, S. R.; Wang, L.-S. *J. Phys. Chem. A* **1997**, *101*, 2103.
(53) Nakajima, A.; Hayase, T.; Hayakawa, F.; Kaya, K. *Chem. Phys. Lett.* **1997**, *280*, 381.
(54) Moravec, V. D.; Klopcic, S. A.; Jarrold, C. C. *J. Chem. Phys.* **1999**, *110*, 5079.
(55) Moravec, V. D.; Jarrold, C. C. *J. Chem. Phys.* **2000**, *113*, 1035.
(56) Moravec, V. D.; Jarrold, C. C. *J. Chem. Phys.* **2000**, *112*, 792.
(57) Chatterjee, B.; Akin, F. A.; Jarrold, C. C.; Raghavachari, K. *J. Chem. Phys.* **2003**, *119*, 10591.
(58) Klopcic, S. A.; Moravec, V. D.; Jarrold, C. C. *J. Chem. Phys.* **1999**, *110*, 8986.
(59) Akin, F. A.; Jarrold, C. C. *J. Chem. Phys.* **2003**, *118*, 1773.
(60) Akin, F. A.; Jarrold, C. C. *J. Chem. Phys.* **2003**, *118*, 5841.
(61) Das, U.; Raghavachari, K.; Jarrold, C. C. *J. Chem. Phys.* **2005**, *122*.
(62) Yoder, B. L.; Maze, J. T.; Raghavachari, K.; Jarrold, C. C. *J. Chem. Phys.* **2005**, *122*.
(63) Dietz, T. G.; Duncan, M. A.; Powers, D. E.; Smalley, R. E. *J. Chem. Phys.* **1981**, *74*, 6511.
(64) Bakker, J. M. B. *J. Phys. E: Sci. Instrum.* **1973**, *6*, 785.
(65) Bakker, J. M. B. *J. Phys. E: Sci. Instrum.* **1974**, *7*, 364.
(66) Campbell, E. E. B.; Levine, R. D. *Annu. Rev. Phys. Chem.* **2000**, *51*, 65.
(67) Surber, E.; Sanov, A. *J. Chem. Phys.* **2003**, *118*, 9192.
(68) Zhao, Y.; de Beer, E.; Xu, C.; Taylor, T.; Neumark, D. M. *J. Chem. Phys.* **1996**, *105*, 4905.
(69) Frisch, M. J. T., G. W.; Schlegel, H. B.; Scuseria, G. E.; Robb, M. A.; Cheeseman, J. R.; Montgomery, J. A., Jr.; Vreven, T.; Kudin, K. N.; Burant, J. C.; Millam, J. M.; Iyengar, S. S.; Tomasi, J.; Barone, V.; Mennucci, B.; Cossi, M.; Scalmani, G.; Rega, N.; Petersson, G. A.; Nakatsuji, H.; Hada, M.; Ehara, M.; Toyota, K.; Fukuda, R.; Hasegawa, J.; Ishida, M.; Nakajima, T.; Honda, Y.; Kitao, O.; Nakai, H.; Klene, M.; Li, X.; Knox, J. E.; Hratchian, H. P.; Cross, J. B.; Bakken, V.; Adamo, C.; Jaramillo, J.; Gomperts, R.; Stratmann, R. E.; Yazyev, O.; Austin, A. J.; Cammi, R.; Pomelli, C.; Ochterski, J. W.; Ayala, P. Y.; Morokuma, K.; Voth, G. A.; Salvador, P.; Dannenberg, J. J.; Zakrzewski, V. G.; Dapprich, S.; Daniels, A. D.; Strain, M. C.; Farkas, O.; Malick, D. K.; Rabuck, A. D.; Raghavachari, K.; Foresman, J. B.; Ortiz, J. V.; Cui, Q.; Baboul, A. G.; Clifford, S.; Cioslowski, J.; Stefanov, B. B.; Liu, G.; Liashenko, A.; Piskorz, P.; Komaromi, I.; Martin, R. L.; Fox, D. J.; Keith, T.; Al-Laham, M. A.; Peng, C. Y.; Nanayakkara, A.; Challacombe, M.; Gill, P. M. W.; Johnson, B.; Chen, W.; Wong, M. W.; Gonzalez, C.; and Pople, J. A. *Gaussian 03*, revision C.02; Gaussian, Inc.: Wallingford, CT, 2004.
(70) Becke, A. D. *J. Chem. Phys.* **1993**, *98*, 5648.
(71) Lee, C.; Yang, W.; Parr, R. G. *Phys. Rev. B: Condens. Matter* **1988**, *37*, 785.
(72) Miehlich, B.; Savin, A.; Stoll, H.; Preuss, H. *Chem. Phys. Lett.* **1989**, *157*, 200.
(73) Bergner, A.; Dolg, M.; Kuechle, W.; Stoll, H.; Preuss, H. *Mol. Phys.* **1993**, *80*, 1431.
(74) Dolg, M.; Stoll, H.; Preuss, H.; Pitzer, R. M. *J. Phys. Chem.* **1993**, *97*, 5852.
(75) Dolg, M.; Wedig, U.; Stoll, H.; Preuss, H. *J. Chem. Phys.* **1987**, *86*, 866.
(76) Schwerdtfeger, P.; Dolg, M.; Schwarz, W. H. E.; Bowmaker, G. A.; Boyd, P. D. W. *J. Chem. Phys.* **1989**, *91*, 1762.
(77) Frisch, M.; Pople, J.; Binkley, J. *J. Chem. Phys.* **1984**, *80*, 3265.
(78) Bauernschmitt, R.; Ahlrichs, R. *Chem. Phys. Lett.* **1996**, *256*, 454.
(79) Casida, M. E.; Jamorski, C.; Casida, K. C.; Salahub, D. R. *J. Chem. Phys.* **1998**, *108*, 4439.
(80) Stratmann, R. E.; Scuseria, G. E.; Frisch, M. J. *J. Chem. Phys.* **1998**, *109*, 8218.
(81) Metz, R. B. *Int. Rev. Phys. Chem.* **2004**, *23*, 79.
(82) Ryan Z. Hinrichs, J. J. S., and H. Floyd Davis. C−C versus C−H bond activation of alkynes by early second-row transition metal atoms. *J. Phys. Chem. A*, submitted.